Materials Chemistry and Physics 138 (2013) 392–398

Contents lists available at SciVerse ScienceDirect

Materials Chemistry and Physics

journal homepage: www.elsevier.com/locate/matchemphys

Electrical and optical properties of copper-complexes thin films grown by the vacuum thermal evaporation technique

M.E. Sánchez-Vergara [a,*], M. Rivera [b], J.C. Alonso-Huitrón [c], A. Rodriguez [c], J.R. Álvarez-Bada [a]

[a] Facultad de Ingeniería, Universidad Anáhuac México Norte, Avenida Universidad Anáhuac 46, Col. Lomas Anáhuac, 52786 Huixquilucan, Estado de México, Mexico
[b] Instituto de Física, Dpto. Materia Condensada, Universidad Nacional Autónoma de México, Coyoacán, 04510 México D.F., Mexico
[c] Instituto de Investigaciones en Materiales, Universidad Nacional Autónoma de México, A. P. 70-360, Coyoacán, 04510 México D.F., Mexico

HIGHLIGHTS

- Thin films of $K_2[Cu(C_2O_4)_2]$] and 1,8-dihydroxyanthraquinone salt were deposited.
- The thin films show electrical conductivities within the range of 10^{-5}–10^{-6} S cm^{-1}.
- The optical gaps associated to the films were determined.
- The PL spectra are influenced by the structure and nature of the organic ligand.

ARTICLE INFO

Article history:
Received 30 March 2012
Received in revised form
30 October 2012
Accepted 25 November 2012

Keywords:
Thin films
Evaporation
Electrical properties
Optical properties

ABSTRACT

In this work, the synthesis and characterization of molecular materials formed from $K_2[Cu(C_2O_4)_2]$, 1,8-dihydroxyanthraquinone and its potassium salt are reported. These complexes have been used to prepare thin films by vacuum thermal evaporation. The synthesized materials were characterized by scanning electron microscopy (SEM), atomic force microscopy (AFM), fast atomic bombardment (FAB+) mass and ultraviolet–visible (UV–vis) spectroscopy. Electrical transport properties were studied by dc conductivity measurements. The electrical activation energies of the complexes, which were in the range of 0.36–0.65 eV, were calculated from their Arrhenius plots. Optical absorption studies in the 100–1100 nm wavelength range at room temperature showed thin films' optical band gaps in the 2.3–3.9 eV range for direct transitions. On the other hand, strong visible photoluminescence (PL) at room temperature was noticed from the thermally-evaporated thin solid films. The PL of all investigated samples were observed with the naked eye in a bright background. The PL and absorption spectra of the investigated compounds are strongly influenced by the molecular structure and nature of the organic ligand.

1. Introduction

The discovery and subsequent success of organic light-emitting diodes led to a tremendous amount of work devoted to understanding optical and transport properties of organic semiconductors [1]. These semiconductors have shown great potential as materials for optoelectronic and electronic devices for solar cells, organic light-emitting diodes (OLED) or optical limiters [2]. The use of organic semiconductors in the fabrication of organic light-emitting devices (OLEDs) has been possible due to the photoluminescence properties of these materials and their films. Of particular interest is the interplay among optical, electronic and morphological properties of OLED materials [3]. For instance, optical properties of organic semiconductors, such as luminescence, are strongly related to the electronic configuration of the valence band and the excitation–deexcitation process between the highest occupied molecular orbitals (HOMO), π, and the lowest unoccupied molecular orbitals (LUMO), π^*. The band gap is the most important parameter in the physics of semiconductors, especially for those widely used in optoelectronic applications [4]. Organic semiconductors exhibit fundamental absorptions in the infrared, visible or ultraviolet spectral regions. The absorption peaks are normally associated with optical transitions through the material band gap. In particular, the phenomenon in which an electronic excitation occurs due to optical transitions is called interband absorption.

In amorphous semiconductors, optical transitions, such as the so-called indirect transitions, are highly favored. These electronic transitions from states in the valence band to states in the conduction band, with no conservation of the electronic

* Corresponding author.
E-mail address: elena.sanchez@anahuac.mx (M.E. Sánchez-Vergara).

0254-0584/$ – see front matter © 2012 Elsevier B.V. All rights reserved.
http://dx.doi.org/10.1016/j.matchemphys.2012.11.072

momentum [5], produce tails in the absorption spectrum within the gap region [6]. Since tails arise as a consequence of the characteristic disorder of these materials, the absorption edge of an amorphous semiconductor is difficult to determine experimentally. As a result, various empirical methods have been developed to measure the optical gap [6]. The most widely used representation is the Tauc model, which assumes that the characteristic disorder of amorphous semiconductors relaxes the momentum conservation rules. This model further argues, taking into account the crystalline–semiconductor nature of the material, that the momentum matrix element is independent of the photon energy ($h\nu$). As a consequence, assuming square-root-like distributions for the valence and conduction band states for sufficiently large values of $h\nu$, one may conclude that an extrapolation of the essentially linear functional dependence of $[\alpha(h\nu)/\beta^2(h\nu)]^{1/2}$ may be observed in amorphous semiconductors. In this case, the optical transition matrix element $\beta^2(h\nu)$ represents the empirical gap [6]. Two parameters that further characterize the Tauc's model are: (1) the mean energy gap, and (2) the energy gap variance, both of them related to the distributions of conduction and valence band states [6]. The mean energy gap parameter (E_g) turns out to be a much more reliable measurement of the fundamental gap than the Tauc gap variance, since the broadening of the absorption spectrum increases with the disorder and decreases with the fundamental gap [6].

Research on molecular electronics involving transition metal complexes has been subject of considerable interest due to the fact that the oxidation states of transition metals can be varied to a great extent by increasing the electron transfer processes [7,8]. The chemistry of stabilized $A_2[TiO(C_2O_4)_2]$ (A = K, PPh_4) complexes is of particular relevance, as these compounds are valuable building blocks in studies of electron transfer processes [9]. Recent research work has been oriented to the formation and characterization of molecular material thin films [10–12]. Transition metal complexes with similar $K_2[TiO(C_2O_4)_2]$ structure dissolved in organic solvents, have been employed to produce -through redox processes- thin films with excellent electrical properties, including the ability to form resilient semiconductor thin films, as well as the capability to undergo molecular and structural modifications. For this reason, the control of these properties has become an important goal in this field [13–15]. The aim of this work was to investigate the electronic structure and energy transfer mechanisms of thin films of copper oxalate complexes. These materials seem to be promising building blocks to obtain multilayered molecular-based materials. In this work, the $K_2[Cu(C_2O_4)_2]$, 1,8-dihydroxyanthraquinone ($C_{14}H_8O_4$) and its potassium salt ($K_2C_{14}H_6O_4$) derivative were used as building blocks to synthesize semiconductor thin films. Thermal evaporation and ellipsometry were employed in the growth and characterization of the films, respectively. The refractive indices and absorption coefficients were determined, since both parameters are of particular interest in the design and fabrication of optoelectronic devices [16,17]. The Tauc band and the electrical conductivity of the resulting thin films were also examined. The surface properties were studied by scanning electron microscopy and atomic force microscopy. Finally, the photoluminescence of the copper thin films was investigated over a wide spectral range at room temperature.

2. Experimental procedure

2.1. Starting materials and chemicals

The raw materials for this work were obtained from commercial suppliers and used without further purification. $K_2[Cu(C_2O_4)_2]$ was obtained from the reaction of $CuSO_4$ with $K_2C_2O_4$ in water. FTIR spectra were acquired with a Perkin Elmer IR spectrophotometer model 282-B using Nujol mulls. Fast atomic bombardment (FAB+) mass spectroscopy of the powder samples was performed on a 3-nitrobenzyl alcohol support in the positive-ion mode on a *JEOL* spectrometer, model *JMS-SX102A*.

Synthesis of material **A**: dissolve 0.23 g (0.71 mmol) of $K_2[Cu(C_2O_4)_2]$ in 10 mL of ethanol for two hours. Then add 0.17 g (0.71 mmol) of 1,8-dihydroxyanthraquinone and keep it in reflux for 72 h. Cool at room temperature, filter and wash with ethanol. The resulting blue powder was dried at high vacuum, yielding 65% of the reaction. m.p. 310 °C (dec). MS(FAB^+, DMSO/EtOH) *m*/*z*: 392 $[Cu(C_2O_4)(C_{14}H_8O_4)]^+$, 241 $[C_{14}H_8O_4]^+$, 240 $[Cu(C_2O_4)_2]^+$.

Synthesis of material **B**: it follows a similar procedure as for material **A**, using 0.23 g (0.71 mmol) of $K_2[Cu(C_2O_4)_2]$ and 0.22 g (0.71 mmol) of potassium salt from 1,8-dihydroxyanthraquinone. Yield 71%. m.p. 300 °C (dec). MS(FAB^+, DMSO/EtOH) *m*/*z*: 392 $[Cu(C_2O_4)(C_{14}H_8O_4)]^+$, 241 $[C_{14}H_8O_4]^+$, 240 $[Cu(C_2O_4)_2]^+$, 39 $[K]^+$.

2.2. Thin film deposition

Thin film deposition of these compounds was carried out by vacuum thermal evaporation onto quartz slices and (100) single-crystalline silicon (c-Si), 200 Ω-cm wafers. The substrate temperatures were kept at 298 K during deposition. The quartz substrates were ultrasonically degreased in warm ethanol and dried in a nitrogen atmosphere. The silicon substrates were chemically etched with a *p-etch* solution (10 ml HF, 15 ml HNO_3 and 300 ml H_2O) in order to remove the native oxide from the c-Si surface. The evaporation source was a molybdenum boat with two grids. The temperature through the molybdenum boat was slowly increased to 453 K, below the first significant signal change observed in the thermo-gravimetric analysis thermogram, in order to prevent thermal decomposition of the compound and to identify the phase transitions such as evaporation, sublimation, etc. All samples were obtained using the same deposition system, with the crucible and substrates arranged in the same geometry. The pressure in the vacuum chamber before the film deposition (1×10^{-4} torr), the amount of mass inside the crucible (0.1 g) and the evaporation time were the same in all cases. In spite of these similarities, significant differences in the thicknesses of the deposited films were detected, which may be related to differences in the sublimation rates of the employed compounds. It is worth mentioning that, although the largest amount of the evaporated materials was found over the substrates, a very tiny quantity was found in the evaporation chamber.

2.3. Thin film characterization

(i) The chemical bonding behavior was analysed by means of a Fourier transform infrared (FTIR) spectrophotometer (Nicolet-210). (ii) A Gaertner L117 Ellipsometer equipped with a He–Ne laser (λ = 632.8 nm) was used to measure the thickness and refractive index of the films. (iii) Ultraviolet–visible (UV–vis) transmission measurements were carried out in the range between 300 and 1100 nm using a double-beam Perkin Elmer Lambda 35 UV–vis spectrophotometer. (iv) Photoluminescence (PL) measurements were carried out in a dark room at room temperature, using a beam (λ = 325 nm, 25 mW) from a Kimmon He–Cd laser as excitation source, with an incident angle of 45° relative to the normal of the sample. The luminescence was collected at an angle normal to the sample using a quartz optical fiber and measured in the range between 350 nm and 800 nm with a Fluoromax-Spex spectrofluorometer. For PL, infrared and ellipsometric measurements of films deposited onto c-Si(100) substrates were used. For optical transmission measurements, bare quartz slices were employed. (v) Conductivity measurements were performed with the four-point

probe method, where quartz slice substrates coated with four metallic strips that acted as electrodes were employed. (vi) The surface morphology of the films was observed with a JEOL5600 scanning electron microscope at 20 kV and the surface morphology and roughness was analysed with a JEOL JSPM4210 atomic force microscope in the tapping mode.

3. Results and discussion

3.1. Thin film structure and morphology

SEM and AFM analysis were performed to investigate the surface coverage, film quality, and composition of the newly formed films. Fig. 1 shows SEM micrographs of materials **A** and **B**. A rough appearance was found in all of them and a very different aspect can be seen in all images. For instance, despite most of the deposits being amorphous in nature, sample **B** exhibits some crystalline forms of different sizes and growth directions. On the other hand, AFM images show a larger magnification of the surface structure. Fig. 2a corresponds to sample **A** deposited onto quartz, while Fig. 2b shows the same material onto c-Si(100). Fig. 2c and d shows films from compound **B** deposited onto quartz and c-Si(100), respectively. Topography obtained by AFM showed RMS roughness values of 72 nm and 66.9 nm for sample **A** onto quartz and c-Si(100), respectively while roughness values of 19.8 nm and 19.4 nm were found for compound **B** onto quartz and c-Si(100), respectively. The difference in roughness between these two samples could be correlated with the type of bidentate ligand in each molecular material [18]. Material **A** onto quartz exhibits an irregular texture with similar but slightly large aggregates and some voids on the surface. Film **A** onto c-Si(100) shows smaller aggregates forming a denser film, although some clear spots can still be seen. Nevertheless, both films exhibit a nearly complete coverage of the substrate and similar film heights. On the other hand, thin films from sample **B** (Fig. 2c and d) exhibit very small aggregates of similar aspect and film heights. In both cases, a total-surface coverage and a fine-film structure can be observed. From the AFM images, it is clear that the substrate does not influence the morphology of the films; rather, it is the chemical structure of the complex that defines the aggregation state on the substrates.

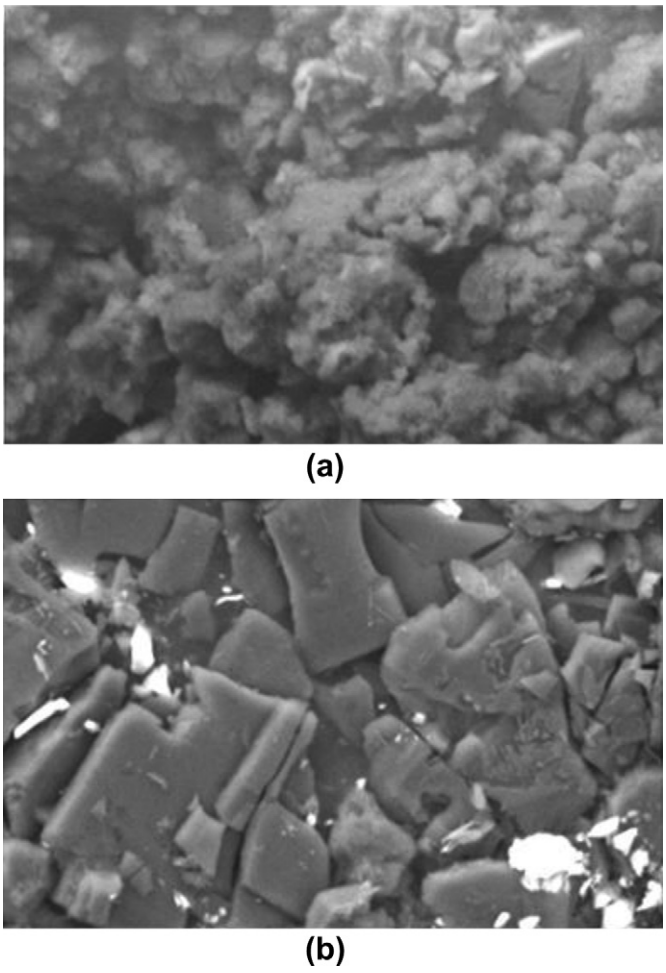

Fig. 1. SEM micrographs of the films from (a) material **A** and (b) material **B** at ×1000.

FTIR spectroscopic measurements were obtained in order to determine significant changes of the raw materials after thermal evaporation. Fig. 3 shows infrared absorption spectra of molecular materials in Nujol mulls. Due to the thermal stability of these compounds, chemical changes or reactions were not expected to occur. Although the deposited material is amorphous in nature, it is formed by the same chemical unit as that in the synthesized powder.

Table 1 shows the characteristic IR bands for the newly synthesized compounds in their different forms: Nujol mulls and films. The slight shifts observed may be due to internal stress produced during the film formation. It is important to notice that the high chemical and thermal stability of the films could make them suitable materials for nanoelectronic applications at temperatures below 453 K. The peaks responsible for carbon–carbon stretching and bending occur at 841 and 814 cm^{-1}. The peak at 1083 cm^{-1} results from a carbon–oxygen stretch within 3338 cm^{-1}. The presence of new aromatic ν(C–H) and ν(C–C) signals around 3070–3040 and 1625–1605 cm^{-1} in samples denotes the attachment of the acceptor 1,8-dihydroxyanthraquinone and its potassium salt. The ν(C=O) and ν(C–O) bands were found around 1670 cm^{-1} and in the range of 3400–3330 cm^{-1}, respectively.

Despite the relatively low solubility of these powder compounds, the positive-ion FAB mass spectra showed signals for $[C_{14}H_8O_4]^+$ (241 m/z) corresponding to **A** and **B** and fragments containing copper, $[Cu(C_2O_4)_2]^+$ (240 m/z), $[Cu(C_2O_4)(C_{14}H_8O_4)]^+$ (392 m/z), confirming the presence of the donor in **A** and **B**. Signals were also found for $[K]^+$ (39 m/z) in **B** spectra. Two approaches might explain the acceptor–donor interaction in these newly synthesized materials. The first explanation suggests the inclusion of the donor into the coordination sphere of copper, $[Cu(C_2O_4)_2(C_{14}H_6O_4)]^{-n}$, as it was proposed for the complex between titanyl oxalate and 3-hydroxyflavone, $[TiO(C_2O_4)_2(C_{15}H_9O_3)_2]^{-4}$ [19]. On the other hand, it might be possible that a multilayer metallic charge-transfer salt was formed with an arrangement somehow similar to that of (BEDT-TTF)$_4$A[Fe(C_2O_4)$_3$] (A = K, NH_4, H_2O), in which successive layers of BEDT-TTF and alternating layers containing **A** and $Fe(C_2O_4)_3^{-3}$ were arranged [20], $(C_{14}H_6O_4)_xK_y[Cu(C_2O_4)_2]\cdot nH_2O$.

3.2. Electric properties

The electrical conductivity of the films was measured in the 273–373 K temperature range. Fig. 4 shows a semiconductor-like behavior for both synthesized materials and conductivity increases with temperature. In ordinary semiconductors, conductivity is also determined by impurity types, their location and concentration, crystal structure, stacking and orbital overlap, among others. In these semiconducting materials, there are two different processes that describe the movement of carriers within the sample. The intramolecular conduction process occurs between the metal atom and the ligands in the complex: electrons can hop

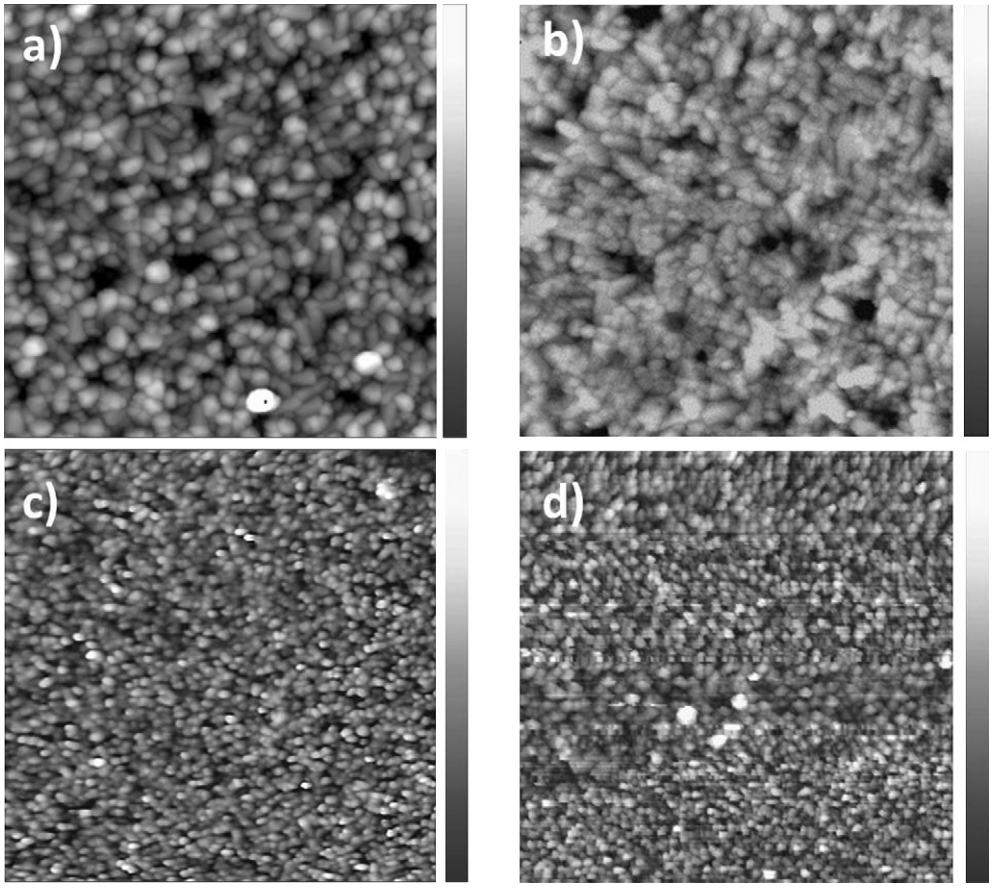

Fig. 2. AFM images of films from compounds **A** and **B** deposited onto quartz and c-Si(100) substrates. (a) **A** onto quartz, (b) **A** onto c-Si(100), (c) **B** onto quartz and (d) **B** onto c-Si(100).

from one atomic site to another if some orbitals exist with the same energy levels. On the other hand, the intermolecular conduction process occurs whenever electrons or holes are capable of traveling from one molecule to another [21]. Calculated values of the electrical conductivity σ at 298 K for all materials under study are summarized in Table 2. These σ values are very similar and lie within the semiconductor region for molecular semiconductors (10^{-6}–10^{2} S cm^{-1}) [13,22]. The significance of these results arises from the fact that a molecular semiconductor is generally defined in terms of its room temperature conductivity and how it changes with temperature.

The dc conductivity has the general form,

$$\sigma = \sigma_0 \exp\left(-\frac{E_a}{kT}\right) \quad (1)$$

where E_a is the thermal activation energy of the electrical conductivity, σ_0 is the pre-exponential factor dependent on the material's nature, and k is Boltzmann's constant. A plot of ln σ versus $1000/T$ yields a straight line whose slope can be used to determine the thermal activation energies of the films [21]. Calculated values of E_a are shown in Table 2. The quantity E_a is an activation energy involving both the energy necessary to excite electrons from the localized states toward extended states through

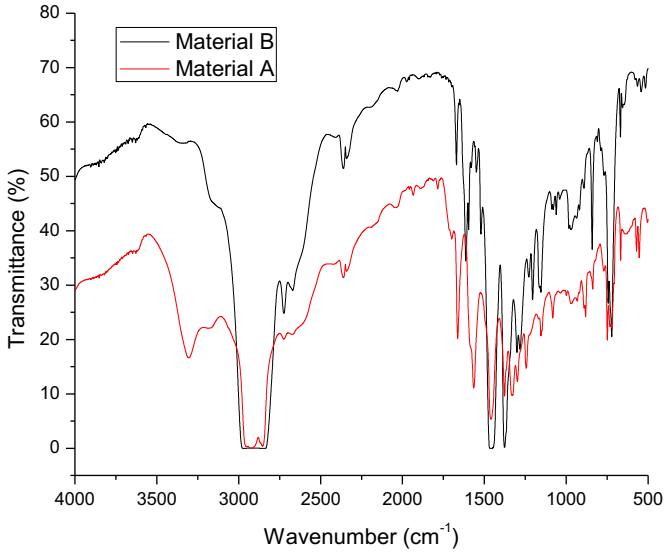

Fig. 3. Infrared absorption spectra of materials **A** and **B**.

Table 1
IR characteristic bands of the synthesized materials for Nujol mulls and thin films (units in cm^{-1}).

Compound	ν(C–C) (cm^{-1})	ν(C=O) (cm^{-1})	ν(C–O) (cm^{-1})
Material **A** Nujol mull	840, 815	1674	3400, 3337, 1083
Material **A** Thin film	835, 814	1672	3403, 3332, 1085
Material **B** Nujol mull	841, 810	1670	3412, 3336, 1084
Material **B** Thin film	839, 815	1673	3410, 3338, 1085

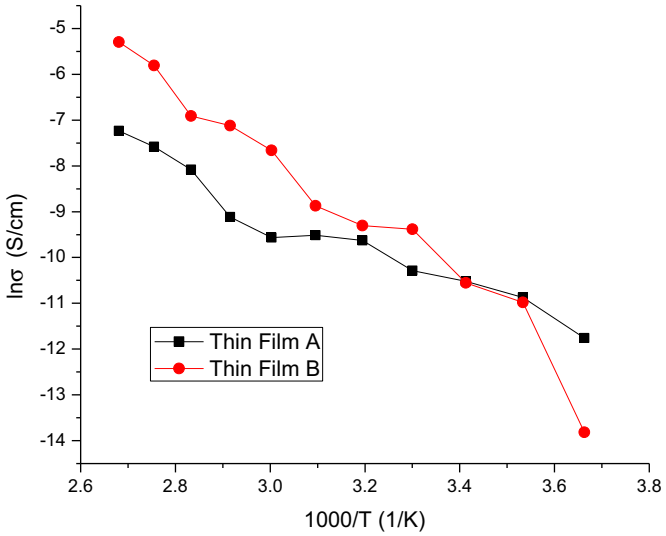

Fig. 4. Temperature dependence of the electrical conductivity of the thin films.

the mobility edge and the electrical conductivity by means of the hopping mechanism between localized states. The lowest activation energy corresponded to the **B** material, which also showed the highest electrical conductivity at room temperature.

3.3. Optical properties

The thicknesses, reflectance percentages and refractive indices of each layer were determined by ellipsometry (see Table 2). Refractive indices and absorption coefficients in semiconductors are relevant in the design and analysis of optoelectronic devices [16]. Some differences in the thickness of the deposited films were detected, which may be related to small differences in the sublimation characteristics of the materials and the bidentate ligand in the compounds.

The optical absorptions of the compounds and the thin films deposited on quartz slices were studied in the 200–1100 nm wavelength range. Fig. 5a shows the graph of absorbance versus wavelength for the **A** and **B** films. Differences on the relative absorbance intensities of the films under examination can be attributed to differences in film thickness and their aggregation state as observed in the AFM-micrographs (see Fig. 2). Furthermore, it was observed that the positions of the absorbance bands were weakly influenced by the backbone structure of these compounds. The band around 350 nm is due to electronic transitions between molecules having an intermediate ionic degree. Spectra for the **A** thin film show a more complicated structure, with optical absorption peaks and edges distributed from the infrared to the ultraviolet regions. It is possible that the bidentate ligand of the potassium salt in the 1,8-dihydroxyanthraquinone molecule may have increased the interfacial distance between $[Cu(C_2O_4)(L)]$

Table 2
Characteristic parameters of materials **A** and **B**.

Optical and electrical parameters	Material **A**	Material **B**
Film thickness (Å)	5727	10,931
Refraction index	2.6	2.3
% reflectance	20.1	15.7
Electrical conductivity (σ) at 298 K (S cm^{-1})	3×10^{-5}	8×10^{-5}
Activation energy (E_a) (eV)	0.65	0.36
Direct Tauc gap (Eg_d) (eV)	3.9	2.3

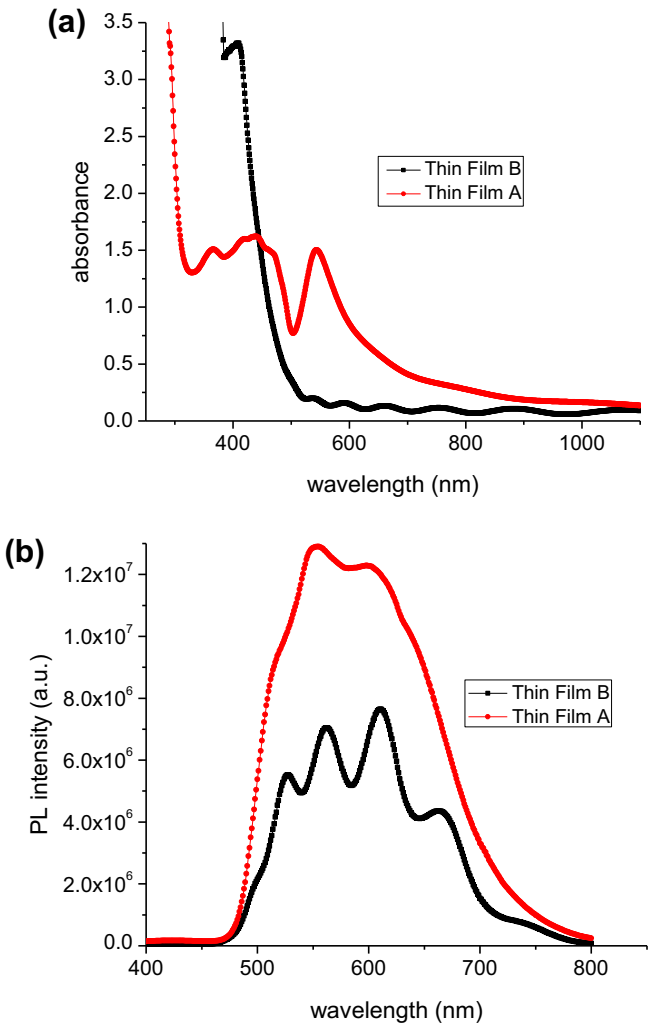

Fig. 5. (a) Absorbance and (b) photoluminescence spectra of thin films **A** and **B**.

groups (material **B**) and therefore a direct overlap of $[Cu(C_2O_4)_2]^+$ is not likely to occur. The absorption bands in the **A** thin film may be interpreted as arising from the overlap of the copper molecule through the 1,8-dihydroxyanthraquinone ligand.

The thickness of the deposited films varies from 5727 to 10,931 Å (see Table 2); hence, the Beer–Lambert law applies for such semi-transparent thin film systems, especially in the case of material **A**. The weak absorption shown within the visible range by the film made from material **A** makes this molecular system an attractive candidate for optical applications due to its transparency at optical wavelengths. Fig. 5b shows the photoluminescence (PL) spectra of the films obtained at room temperature (300 K). It is clear from this figure that these films exhibit an intense luminescence in the visible region. The PL emitted by the excitation spot on the film **A** appeared in the yellow–orange interval and the highest intensity peak occurs at 550 nm (yellow). This emission is observed when a regular ultraviolet lamp is employed. For the **B** film, the emission is in the yellow-to-red interval and the highest intensity peak is observed at 608 nm (orange–red); this emission can be observed with the naked eye while using a regular ultraviolet lamp.

The emission observed in these materials originates basically from direct transitions. This result can be confirmed when a direct

comparison between the maximum emission peaks (for both materials, **A** and **B**) and the calculated optical gap is carried out (the optical gap for compound **B** is around 2.033 eV while the optical gap for compound **A** is 2.25 eV). A larger emission is observed in compound **A** than in compound **B** regardless of the film thickness. Although the film thickness for the **A** compound is half that of film **B**, its integrated emission is almost twice as large as the value for film B. On the other hand, some interference effects due to the films thickness can be seen in the PL emissions from both compounds. These results are of particular interest since they show that compound **A** can be an ideal candidate for further *electroluminescence* tests and possible OLED applications [2].

The band gap is deduced from the UV–vis absorption spectrum according to the semi-empirical Tauc model, which can help to determine the optical band gap in semiconductor amorphous materials [4]. The Tauc optical gap can be obtained from the straight line of the UV–vis absorption spectrum, which is extended toward the *x*-axis. The intercept value corresponds to the optical band gap value [6]. The absorption coefficient α near the band edge in many amorphous semiconductors shows an exponential dependence upon photon energy usually following the empirical relation [23]:

$$\alpha h\nu = \beta(h\nu - E_g)^n \tag{2}$$

In this equation, β^{-1} is the band edge parameter and n is a characteristic number related to the type of transition process. For allowed direct transitions, $n = ½$. Thus, the optical gaps for both transitions could be determined by the extrapolation to zero of the linear regions of the $(\alpha h\upsilon)^2 = f(h\nu)$ curves, Eg_d (Table 2) [23]. The absorption coefficient (α) is defined by the Beer–Lambert law and can be calculated from the optical transmittance [4].

$$\alpha = -\ln T/t \tag{3}$$

T is the transmittance and it is related to the absorbance A according to $A = -\log(T)$; t is the film thickness. Whereas the optical gap can be measured by optical absorption spectroscopy, the transport gap can be measured by ultraviolet or inverse photoemission spectroscopy. The transport gap is larger than the optical gap by a quantity equal to the binding energy of the Frenkel excitons. Fig. 6 exhibits the absorption curves of the samples that show evidence for direct transitions. In amorphous semiconductors there is no conservation of the electronic momentum, since the optical transitions are basically indirect transitions from states in the valence band to states in the conduction band [5]. However, as can be seen in Fig. 6 for the direct transition, the squared absorption coefficient is a linear function of the incident photon's energy, which can be related to the one-electron theory of Bardeen et al. [24,25]. This theory has been successfully applied to analyse the absorption edge of different amorphous semiconductors. The absorption ($\alpha > 10^4$ cm^{-1}) is related to direct interband transitions where the lowest part of the valence band and the highest part in the conduction band share the same wave vector and there is an allowed transition across the band gap. The visible photoluminescence in the thin films is related to such direct transitions.

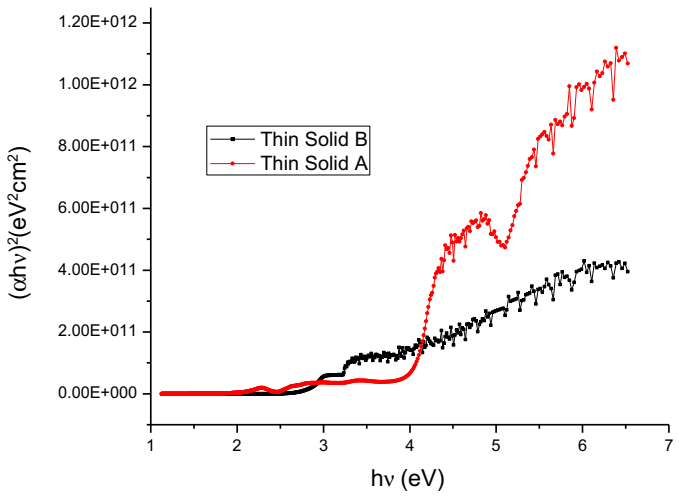

Fig. 6. Absorption curves showing transitions that correspond to direct band gaps.

The direct Tauc gap values of thin films of materials **A** and **B** were found to be 3.9 and 2.3 eV, respectively. The Tauc optical gap is smaller for thicker films, in contrast to its thinner counterpart (see Table 2). A direct comparison between the different properties of the **A** and **B** films shows that material **B** has the smallest band gap and thus the largest conductivity of the two. This behavior is expected if one takes into account that hierarchy factors most likely affect the size of the band gap. Apparently, the potassium in the salt leads to an increase in the charge transport. It is possible that the electronic transport arises from a columnar disposition of the $K_2[Cu(C_2O_4)_2]$-ligand arrangement where the charge transport takes place; the conduction mechanism is mainly associated to the bidentate ligand. This is important because the potassium atom is large (compared with the hydrogen atom in the 1,8-dihydroxyanthraquinone species), and therefore provides a larger electronic delocalization and better electronic transport.

4. Conclusions

Thin films of $K_2[Cu(C_2O_4)_2]$] and 1,8-dihydroxyanthraquinone and its potassium salt were deposited by vacuum thermal evaporation onto different substrates. According to the IR spectra, they exhibit the same chemical units as those of the corresponding synthesized powders. The thin films of the synthesized molecular materials show electrical conductivities at room temperature around 10^{-5} S cm^{-1} and an electrical conductivity increase with temperature which suggests a semiconducting behavior. It was also found that the temperature-dependent electric current is always higher for the voluminous bidentate ligand with large molecular weights. From the Tauc model, the optical gaps associated to the films were determined. The optical transitions were found to be of direct nature. It was also noticed that the PL absorption spectra and surface morphology were strongly influenced by the compounds' molecular structures. From the optical band gap values and the easy preparation of these compounds as thin films, they may have potential applications in the fabrication of nanoelectronic devices.

Acknowledgments

The authors wish to thank the technical assistance of Verónica García (IQ-UNAM). One of the authors (M.E. Sánchez-Vergara) gratefully acknowledges the financial support of the SEP-CONACYT-México project number 153751. M.R. acknowledges the Central Microscopy Laboratory at IF-UNAM for the microscope facilities, and all authors acknowledge Mario Monroy (Ch. Eng.) for SEM technical assistance.

References

[1] M.E. Sánchez-Vergara, O.G. Morales-Saavedra, F.G. Ontiveros-Barrera, V. Torres-Zuñiga, R. Ortega-Martínez, A. Ortiz-Rebollo, Mater. Sci. Eng. B 158 (2009) 98.
[2] W. Freyer, C.C. Neacsu, M.B. Raschke, J. Luminescence 128 (2008) 661.
[3] N. Peltekis, B.N. Holland, S. Krishnamurthy, I.T. McGovern, N.R.J. Poolton, S. Patel, C. McGuinness, J. Am. Chem. Soc. 130 (2008) 13008.

[4] X. Li, H. Zhu, J. Wei, K. Wang, E. Xu, Z. Li, D. Wu, Appl. Phys. A. Mater. Sci. Process. 97 (2009) 341.
[5] G.D. Cody, Hydrogenated amorphous silicon, part B, optical properties, in: J.I. Pankove (Ed.), Semiconductors and Semimetals, vol. 21, Academic Press, Orlando, 1984.
[6] S.K. O'Learly, P.K. Lim, Solid State Commun. 104 (1) (1997) 17.
[7] D. Astruc, Acc. Chem. Res. 30 (1997) 383.
[8] H.E. Toma, J. Braz. Chem. Soc. 14 (2003) 845.
[9] P. Ganguly, D.V. Paranjape, M. Sastry, Langmuir 9 (1993) 577.
[10] P. Cassoux, D. De Caro, L. Valade, H. Casellas, B. Daffos, M.E. Sánchez Vergara, Mol. Cryst. Liq. Cryst. Sci. Technol., Sect. A 380 (2002) 45.
[11] J. Caro, S. Garelik, A. Figeras, Chem. Vap. Deposition 2 (1996) 251.
[12] A. Figueras, J. Cryst. Growth 166 (1996) 798.
[13] S.J. Kim, M. Matsumoto, K. Shigehara, J. Porphyrins Phthalocyanines 4 (2000) 136.
[14] P.L. Boulas, M. Gomez-Kaifer, L. Echegoyen, Angew. Chem. Int. Ed. 37 (1998) 216.
[15] A. Cázares-Sánchez, M.E. Sánchez-Vergara, J. Chavez-Carvayar, B. Frontana-Uribe, C. Álvarez Toledano, Científica 3 (2003) 15.
[16] M. Sridharan, S.K. Narayandass, D. Mangalaraj, J. Mater. Sci.: Mater. Electr. 13 (2002) 471.
[17] P.N. Prasad, D.J. Williams, Introduction to Nonlinear Optical Effects in Molecules and Polymers, Wiley Interscience, New York, 1991 (Chapter 1).
[18] L. Ottaviano, S. Di Nardo, L. Lozzi, M. Passacantando, P. Picozzi, S. Santucci, Surf. Sci. 373 (1997) 318–332.
[19] M. Aleksic, S. Blagojevic, D. Malesec, Z. Radovic, J. Serb. Chem. Soc. 65 (2000) 631.
[20] M. Kurmoo, A.W. Graham, P. Day, S.J. Coles, M.B. Hurtshouse, J.L. Caulfield, J. Singleton, F.L. Pratt, W. Hayes, L. Ducasse, P. Guionneau, J. Am. Chem. Soc. 117 (1995) 12209.
[21] S. Sarkar, Y. Aydogdu, F. Dagdelen, B.B. Bhaumik, K. Dey, Mater. Chem. Phys. 88 (2004) 357.
[22] M.S. Kiani, G. RMitchell, Synth. Met. 46 (1992) 293.
[23] F. Urbach, Phys. Rev. 92 (1953) 1434.
[24] M.M. El-Nahass, K.F. Abd-El-Rahman, A.A. Al-Ghamdi, A.M. Asiri, Phys. B 344 (2004) 398.
[25] J. Bardeen, F.J. Slatt, L.J. Hall, in: Photoconductivity Conference. Wiley, New York, 1956, p. 146.